Spectral Functions of Isolated Ce Adatoms on Paramagnetic Surfaces

S. Gardonio,[1,2] T. O. Wehling,[3] L. Petaccia,[2] S. Lizzit,[2] P. Vilmercati,[2] A. Goldoni,[2]
M. Karolak,[3] A. I. Lichtenstein,[3] and C. Carbone[4]

[1]*University of Nova Gorica, Vipavska 11c, 5270 Ajdovscina, Slovenia*
[2]*Sincrotrone Trieste SCpA, Strada Statale 14, Km. 163.5, 34149 Trieste, Italy*
[3]*I. Institut für Theoretische Physik, Universität Hamburg, Jungiusstraße 9, D-20355 Hamburg, Germany*
[4]*Istituto di Struttura della Materia, Consiglio Nazionale delle Ricerche, Trieste, Italy*

(Received 4 January 2011; revised manuscript received 25 April 2011; published 5 July 2011)

We report photoemission experiments revealing the full valence electron spectral function of Ce adatoms on Ag(111), W(110), and Rh(111) surfaces. A transfer of Ce $4f$ spectral weight from the ionization peak towards the Fermi level is demonstrated upon changing the substrate from Ag(111) to Rh(111). In the intermediate case of Ce on W(110) the ionization peak is found to be split. This evolution of the spectra is explained by means of first-principles theory, which clearly demonstrates that a reliable understanding of magnetic adatoms on metal surfaces requires simultaneous low and high energy spectroscopic information.

DOI: 10.1103/PhysRevLett.107.026801 PACS numbers: 73.20.Hb, 73.22.−f, 75.75.Lf, 79.60.−i

Ce atoms coupled to a metallic host present a characteristic case of quantum impurity problems: The competition of strong Coulomb interactions of the Ce $4f$ electrons and hybridization effects puts these states at the borderline between localized and delocalized. Hence, the physics of Ce compounds or Ce impurities in metallic hosts ranges from local moment behavior in weakly hybridizing environments to nonmagnetic Ce in the case of strong hybridization and rich Kondo physics in between [1,2]. To date, there are two experimental techniques allowing us to probe the spectral properties of such systems: scanning tunneling spectroscopy (STS) and photoemission (PE) techniques (see [2,3] for recent reviews).

Advances in nanotechnology like the ability of controlled atom manipulation have put the electronic properties of magnetic nanosystems into the focus of intense research: STS is well suited to studying individual magnetic atoms on surfaces within a spectral range of some few 100 meV around the Fermi level and with very high spatial resolution. Starting in 1998, these techniques revealed how magnetic adatoms give rise to a sharp Abrikosov-Suhl resonance in the vicinity of the Fermi level—a characteristic fingerprint of the Kondo effect [4,5]. However, higher energy spectral properties ($4f$ or $3d$ ionization peaks and/or corresponding crystal-field-split states) are difficult to obtain with STS and one is restricted to the analysis of the Kondo resonance close to the Fermi energy. A test of the resulting Anderson model parameters with higher-lying levels is hardly possible. PE, on the contrary, can resolve spectra in the full range of the valence band but has so far been limited mainly to the study of Ce alloys (see [2,6] for reviews). Measuring the full spectral properties of isolated magnetic adatoms on transition metal surfaces remains, therefore, an open experimental challenge.

In this Letter, we extend the energy range in which the spectral properties of magnetic adatoms on metallic surfaces can be probed. We report on photoemission experiments revealing the full valence band electronic structure of isolated Ce adatoms on the surfaces of Ag(111), W(110), and Rh(111) and fully describe the valence band electronic structure of isolated Ce adatoms on these different hosts. For the first time, our studies reveal the $4f$ ionization peaks and the Kondo excitations for isolated Ce adatoms on a metallic surface in a single experiment. By means of first-principles calculations we explain the photoemission results and yield the link between the atomistic environment of the Ce adatoms and their spectroscopic properties.

We prepared the Ag(111), W(110), and Rh(111) substrates by the standard procedures and monitored their crystalline quality by low energy electron diffraction (LEED). The LEED pattern quality was very high, with sharp diffraction spots on low background, for all three substrates. Isolated adatoms were obtained by depositing Ce atoms at a substrate temperature of 20 K (statistical growth regime). The Ce coverages were calibrated by a quartz microbalance and cross-checked by the known LEED pattern for submonolayer Ce deposited on W(110) [7]. The sample temperature was maintained at 20 K during the photoemission measurements. A major technical difficulty in photoemission experiments on isolated magnetic adatoms on metal surfaces (requiring adatom coverages in the range of 10^{-2}–10^{-3} ML) is that the spectroscopic signature of the adatoms can be obtained only for those combinations of impurities and substrates for which the signal of the impurity is comparable to the host. We demonstrate that this condition is fulfilled for photoemission measurements of $4f$ valence states of rare earth isolated atoms on transition and noble metal surfaces

 © 2011 American Physical Society

measured across the $4d \rightarrow 4f$ threshold (resonant photoemission). Here, the required sensitivity to the adatoms is achieved because of the enhanced photoemission cross section of the $4f$ states as compared to the $3d$, $4d$, or $5d$ photoemission cross sections of the transition and noble metal substrates. The photoemission experiments were performed at the SuperESCA beam line at the Elettra synchrotron radiation facility. We measured photoemission energy distribution curves of the Ce $4f$ valence state at 122 eV photon energy, which corresponds to Ce $4d \rightarrow 4f$ resonance, with an overall energy resolution of 40 meV.

Figure 1 shows the resonant photoelectron spectra measured at the Ce $4d \rightarrow 4f$ absorption threshold for isolated Ce atoms on Ag(111), W(110), and Rh(111) surfaces. In order to better distinguish between the photoemission signal derived from the Ce adatoms and the substrate contribution, the photoemission spectra before (a) and after (b) deposition of the Ce atoms are compared and the difference spectra (c) are taken for each host. The spectra of isolated Ce atoms are found to be markedly different on the three substrates and a clear trend when going from Ag to Rh is visible: On Ag(111) only a peak around -2.9 eV is present, while on W(110) peaks at energies of -1.5 and -2.3 eV as well as two smaller peaks close to the Fermi level, at 0 and -0.25 eV, contribute spectral weight. On Rh(111) the major contribution is derived from structures close to the Fermi level, the peaks labeled 1 and 2, and a small broad peak around -2.3 eV is still present. The $4f$ electrons of Ce seem to undergo a transition from localized to delocalized when going from Ce on Ag(111) to Ce on Rh(111) via the intermediate case of Ce on W(110) where the ionization peak appears to be split up into two peaks.

To understand the origin of these entirely different distributions of Ce $4f$ spectral weight and to explain why the ionization peak is split up on W(110), we proceeded in two steps. First, density functional theory (DFT) calculations are performed to obtain relaxed geometries and the hybridization functions for single Ce atoms on Ag(111), W(110),

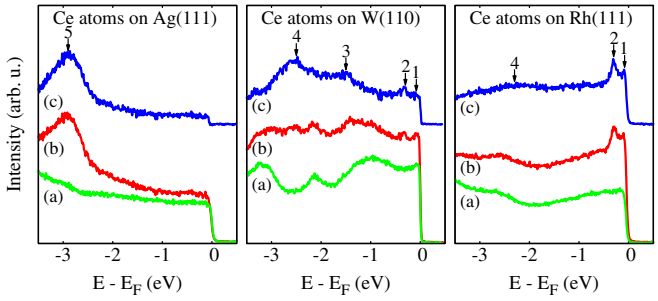

FIG. 1 (color online). Valence photoelectron energy distribution curves for the clean Ag(111), W(110), and Rh(111) surfaces (a) and in the presence of 0.005 ML, 0.0075 ML, and 0.003 ML of Ce, respectively. These coverages correspond to statistically distributed isolated atoms (b). The curves (c) are the differences between the spectra (b) and (a). All energies E are given relative to the Fermi level E_F.

and Rh(111). These hybridization functions are afterwards used to calculate the valence electron photoemission spectra following Gunnarsson and Schönhammer [8]. The DFT calculations have been carried out using a generalized gradient approximation (GGA) [9] as implemented in the Vienna *ab initio* simulation package (VASP) [10] with the projector augmented waves basis sets [11,12]. In these calculations, single Ce atoms on Ag(111), W(110), and Rh(111) have been modeled using 2×2 surface supercells with slab thicknesses of 7 layers. The crystal structures have been relaxed until the forces acting on each atom were less than 0.02 eV/Å. In all cases, Ce adsorbs to high symmetry positions, which are close to the continued bulk lattice on Ag(111) and W(110). On the Rh(111) surface, Ce adsorption to an hcp site is by $\sim$250 meV more favorable than the fcc site.

The Ce $4f$ electrons are expected to be subject to strong correlations which require a description in terms of an LDA + + approach [13,14]: For the description of the Ce adatoms we choose Anderson impurity models with the hybridization functions, $\Delta_{mm'}(\omega)$, being obtained from DFT. Here, m, $m' = -3, \ldots, 3$ label the z component of the angular momentum of the Ce $4f$ orbitals. The projector augmented waves basis sets provide intrinsically projections onto localized atomic orbitals, which we use to extract the hybridization functions (for details see [14,15]).

These hybridization functions act like energy dependent complex valued potentials on the Ce f orbitals and fully characterize their interaction with the substrate as regards local observables like the Ce $4f$-spectral functions probed in the photoemission experiments. We obtain the full hybridization function matrices, $\Delta^{\mathrm{GGA}}_{mm'}(\omega)$, from our DFT calculations. Because of the reduced symmetry at the surfaces there are fewer degeneracies than for Ce impurities in bulk metals and off-diagonal matrix elements occur. The off-diagonal elements are comparable in order of magnitude but generally smaller than the diagonal matrix elements. The variations of the diagonal matrix elements $\Delta^{\mathrm{GGA}}_{mm}(\omega)$ with the orbital index m are comparable to the variation between different degenerate blocks in the case of Ce impurities in bulk metals. Hence, we follow Ref. [8] and assume $\Delta_{mm'}(\omega) = \Delta(\omega)\delta_{mm'}$, which we obtain by averaging over all Ce $4f$ orbitals, $\Delta(\omega) = \frac{1}{7}\sum_m \Delta^{\mathrm{GGA}}_{mm}(\omega)$. The resulting $\Delta(\omega)$ for Ce on the three different substrates are shown in Fig. 2(a).

The imaginary part of the Ce $4f$ hybridization, $\mathrm{Im}\Delta(\omega)$, on the Ag(111) is at all energies below the Fermi level more than an order of magnitude smaller than the corresponding $4f$ hybridizations of Ce on W(110) or Rh(111). Obviously, Ce on Rh(111) exhibits by far the strongest hybridization, which gives the first hint why the ionization peak of Ce on Rh(111) is more strongly smeared out and why the quasiparticle peak at the Fermi level might be strongest for Ce on Rh(111). Ce on W(110) presents an intermediate case.

Using Eqs. (A1–A7) from Ref. [8], we obtain the ground state properties of the Ce $4f$ electrons including the energy gain δ upon hybridization and the average occupancy n_f as well as the valence electron photoemission spectra from the hybridization functions. Here, only the on-site f energy remains as a fitting parameter [16], while we use the established value of 252 meV for the spin-orbit splitting between the $f_{5/2}$ and $f_{7/2}$ states. The approach used here is often referred to as first-order expansion. Expansions to higher orders or including double occupancy of the impurity are possible [8]. Such approaches can yield more accurate spectral functions and become particularly important, e.g., in the case of inverse photoemission spectroscopy. For PE experiments as considered here the first-order expansion has been proven to be qualitatively correct [8].

Figures 2(b)–2(d) show the calculated Ce $4f$ spectra for all substrates and different on-site energies ϵ_f. The spectra of Ce on Ag(111) exhibit one sharp peak close to the bare f-electron energy, which corresponds to the ionization process $f^1 \rightarrow f^0$. Independent of ϵ_f the spectral weight of this main peak dominates the spectrum and is by orders of magnitude larger than the weight of a possible Kondo peak: within the entire range of ϵ_f considered in Figs. 2(b)–2(d) we find $1 - n_f < 10^{-4}$. This represents a measure for the weight Z of the Kondo peak, as $Z = 1 - n_f$ for vanishing spin-orbit splitting $\Delta\epsilon_f = 0$ [1,8].

For the case of Ce on Rh(111), the Kondo or the spin-orbit peak ($f_{5/2} \rightarrow f_{7/2}$ around the energy $-\Delta\epsilon_f$) dominates the spectrum for all ϵ_f shown in Figs. 2(b)–2(d) and the ionization peak is always broadened to a wide continuum. Here, the main effect of changing ϵ_f is changing the relative weight of the spin-orbit peak as compared to the Kondo peak.

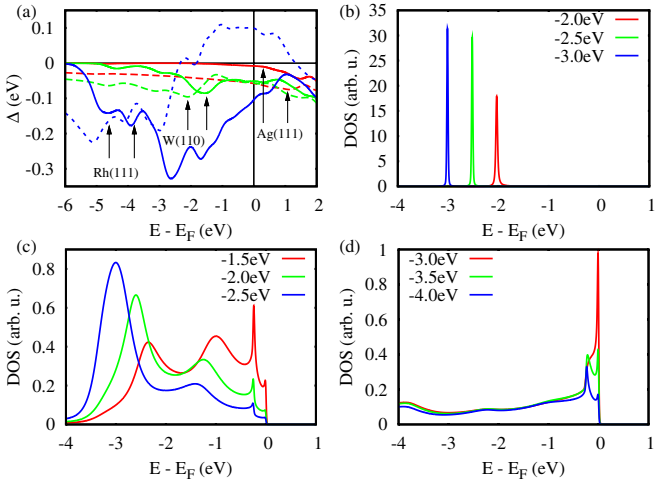

FIG. 2 (color online). (a) Calculated Ce 4 f-electron hybridization functions for isolated adatoms on Ag(111) (red), W(110) (green), and Rh(111) (blue). The real parts are shown as dashed and the imaginary parts as solid lines. (b–d) Calculated $4f$ spectra for single Ce atoms on Ag(111) (b), W(110) (c), and Rh(111) (d) surfaces. The dependence of the spectra on the on-site energies ϵ_f is illustrated by showing spectra obtained with different ϵ_f. All curves are labeled by the corresponding ϵ_f.

The spectra of Ce on W(110) lie in between these two extreme cases with the ionization peak being remarkably split up into two separate peaks at $E > -1.5$ eV and $E < -2.3$ eV in all cases. In this intermediate regime, the on-site-energy strongly affects the ratio of spectral weight in the ionization peak to the amount of weight in the Kondo and the spin-orbit peaks.

The comparison of experimental and theoretical spectra (Fig. 3) shows that theory and experiment are in very good agreement. This suggests that the physical processes determining the photoemission spectra of isolated Ce adatoms on the different surfaces are well described within our model. We now analyze the physical mechanisms behind the diversity of experimentally observed PE spectra.

The adsorption geometries already give a first hint on the origin of the very different hybridization strengths of the Ce adatoms: The heights of Ce above nearest substrate atoms beneath are 2.35 Å on Ag(111), 2.25 Å on W(110), and 1.88 Å on Rh(111). This is well in line with the hybridization strength strongly increasing from Ag(111) to Rh(111) with W(110) as an intermediate case. Particularly the substrate d electrons play an important role in determining the Ce hybridization strengths (Fig. 4). In Ag, the d states are more than 3 eV below the Fermi level, very localized, and there is only a very small contribution from the Ag d states to the Ce hybridization function [$-\mathrm{Im}\Delta(\omega) < 0.01$ eV in the energy range of the Ag d states]. This is very different for W and Rh, which have open d shells and correspondingly d bands extending from ~ -5 eV up to energies well above the Fermi level. The structure of the hybridization functions of Ce on W (110) and Rh(111) follows in both cases the local density of states (LDOS) of the substrate d orbitals, which indicates that the W and Rh d orbitals hybridize considerably stronger with the Ce $4f$ orbitals than in the case of Ag.

In the case of Ce on W(110), there is a peak in $\mathrm{Im}\Delta(\omega)$ extending from $\omega = -1$ to -2 eV. This resonance is caused by bonding to t_{2g} d orbitals of neighboring W atoms. The real parts of the Ce $4f$ hybridization functions

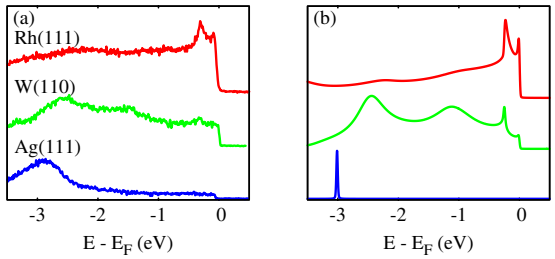

FIG. 3 (color online). Comparison of experimental (a) and theoretical spectra (b). The theoretical spectra present best fits to the experiment obtained with $\epsilon_f = -3$ eV, -1.7 eV, and -3.7 eV for Ce on Ag(111), W(110), and Rh(111), respectively.

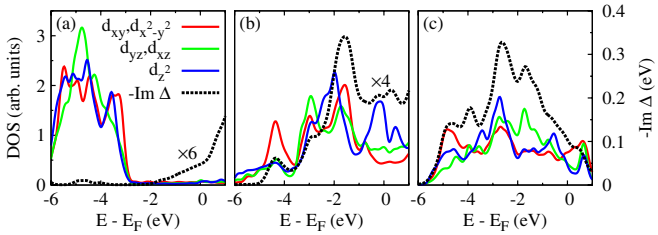

FIG. 4 (color online). d-electron LDOS of substrate atoms which are neighbors of Ce and the Ce $4f$ hybridization functions. For W(110) (b) and Rh(111) (c) the Ce hybridization function follows the shape of the d-electron LDOS of the neighboring atoms—in contrast to Ce on Ag(111) (a).

are related to $\mathrm{Im}\Delta(\omega)$ by the Hilbert transform $\mathrm{Re}\Delta(\omega) = -\frac{1}{\pi}\mathcal{P}\int d\omega' \frac{\mathrm{Im}\Delta(\omega')}{\omega-\omega'}$. Hence, peaks in the imaginary part cause steps in the real part.

On the ionization peak, the hybridization acts like a self-energy term on a resonant level with the real part shifting the level and the imaginary part broadening it. The step in $\mathrm{Re}\Delta(\omega)$ in the energy range of -2.1 to -1.3 eV for Ce on W(110) due to the resonance near $\omega = -1.6$ eV causes spectral weight being shifted to lower energies below the resonance and to higher energies above it. Hence, the resonance in the hybridization function of Ce on W(110) is responsible for the peak splitting observed in photoemission (see Fig. 1).

The Ag(111) and Rh(111) surfaces are forming the two extreme cases of weak and strong hybridization, respectively, and lead to correspondingly sharp or broad ionization peaks. For Ce on Rh(111), there is an even larger step in $\mathrm{Re}\Delta(\omega)$ extending from $\omega = -3$ to -2 eV [Fig. 2(a)]. This large step results in a significant amount of weight being pushed to such high energies that it contributes to the peaks close to the Fermi level but does not form a second separate ionization peak as in the case of Ce on W(110). This effect occurring in the case of strong hybridization has been similarly observed in the bulk compound $CeNi_2$ [1,17]. As in the case of bulk alloys [17], the hybridization of the Ce $4f$ states with the conduction electron states can induce strong structures in the Ce $4f$-spectral function for isolated atoms on surfaces. All experimentally observed trends including the peak splitting in the case of Ce on W (110) are understandable from the structure of the hybridization functions shown in Fig. 2(a).

For the case of Ce on Ag(111), photoemission and theory found concordantly no significant Kondo-like contribution to the spectra. This is in contrast to the Kondo effect of Ce on Ag(111) reported in early STM experiments [5]. The Kondo temperature $T_K = 5$ K $= 0.4$ meV$/k_B$ reported there is out of the range $T_K \sim \delta \ll 10^{-2}$ meV for all $\epsilon_f < 1$ eV found here by combining photoemission and first-principles calculations. Hence, our results support the conjecture (cf. Ref. [3]) that the STM experiments from Ref. [5] have been measuring Ce clusters on Ag(111).

In conclusion, we demonstrated the ability of photoemission spectroscopy to measure the full valence electron spectral function of *isolated* Ce adatoms on different metallic surfaces. By comparing the experimental results with first-principles calculations of the photoemission spectra for the atoms deposited on Ag(111), W(110), and Rh(111) surfaces, we find delocalization of the Ce $4f$ electrons when going from Ag to Rh substrates and observe the shift of spectral weight from the ionization peaks to quasiparticle resonances at the Fermi level. The intermediate case of Ce on W(110) shows that the energy dependence of the impurity hybridization with the surface determines the shape of excitation spectra. Widening the energy window for probing the electronic structure of magnetic nanosystems appears to be a powerful way to disentangle hybridization mechanisms and to understand the physics of magnetic nanosystems down to the atomic level.

We acknowledge financial support through the Italian MIUR Grant No. PRIN 20087NX9Y, SFB 668 (Germany), as well as computer time at HLRN.

[1] A. C. Hewson, *The Kondo Problem to Heavy Fermions* (Cambridge University Press, Cambridge, England, 1993).
[2] J. W. Allen, J. Phys. Soc. Jpn. **74**, 34 (2005).
[3] M. Ternes, A. J. Heinrich, and W.-D. Schneider, J. Phys. Condens. Matter **21**, 053 001 (2009).
[4] V. Madhavan *et al.*, Science **280**, 567 (1998).
[5] J. Li *et al.*, Phys. Rev. Lett. **80**, 2893 (1998).
[6] D. Malterre, M. Grioni, and Y. Baer, Adv. Phys. **45**, 299 (1996).
[7] C. Gu, X. Wu, C. G. Olson, and D. W. Lynch, Phys. Rev. Lett. **67**, 1622 (1991).
[8] O. Gunnarsson and K. Schönhammer, Phys. Rev. B **28**, 4315 (1983).
[9] J. P. Perdew *et al.*, Phys. Rev. B **46**, 6671 (1992).
[10] G. Kresse and J. Hafner, J. Phys. Condens. Matter **6**, 8245 (1994).
[11] G. Kresse and D. Joubert, Phys. Rev. B **59**, 1758 (1999).
[12] P. E. Blöchl, Phys. Rev. B **50**, 17 953 (1994).
[13] A. I. Lichtenstein and M. I. Katsnelson, Phys. Rev. B **57**, 6884 (1998).
[14] M. Karolak *et al.*, J. Phys. Condens. Matter **23**, 085 601 (2011).
[15] B. Amadon *et al.*, Phys. Rev. B **77**, 205112 (2008).
[16] When extracting the parameters of an effective Anderson impurity model from a DFT calculation a double-counting term has to be included in the on-site energy ϵ_f to correct for the Coulomb interactions and electron correlations within the Ce-$4f$ space which are already contained in the DFT. As this double-counting term is not known exactly [15], we leave ϵ_f as an adjustable parameter.
[17] J. W. Allen *et al.*, Adv. Phys. **35**, 275 (1986).